Influence of saturated water content on estimating soil hydraulic properties from cumulative disc infiltrometer measurements

D. Moret-Fernández, F. Lera, D. Yilmaz, Laurent Lassabatère, J.J. Jiménez, B. Latorre

Geoderma 452 (2024) 117089

Contents lists available at ScienceDirect

Geoderma

journal homepage: www.elsevier.com/locate/geoderma

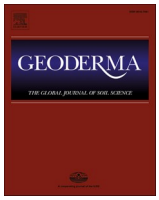

Influence of saturated water content on estimating soil hydraulic properties from cumulative disc infiltrometer measurements

D. Moret-Fernández [a,*], F. Lera [b], D. Yilmaz [c], L. Lassabatere [d], J.J. Jiménez [e], B. Latorre [a]

[a] Departamento de Suelo y Agua, Estación Experimental de Aula Dei, Consejo Superior de Investigaciones Científicas (CSIC), PO Box 13034, 50080 Zaragoza, Spain
[b] Instituto de Investigación en Ingeniería de Aragón, University of Zaragoza, 50018 Zaragoza, Spain
[c] Univ. Grenoble Alpes, CNRS, IRD, Grenoble INP, IGE, 38000 Grenoble, France
[d] Université Claude Bernard Lyon 1, LEHNA UMR 5023, CNRS, ENTPE, F-69518, Vaulx-en-Velin, France
[e] Instituto Pirenaico de Ecología, Consejo Superior de Investigaciones Científicas (IPE-CSIC), Avda. Ntra. Sra. De la Victoria, 16, Jaca 22700, Spain

ARTICLE INFO

Keywords:
Sorptivity
Hydraulic conductivity
Infiltration curve
Inverse analysis
Saturated water content

ABSTRACT

The soil sorptivity, S, and saturated hydraulic conductivity, K_s, are fundamental soil hydraulic properties that can be estimated from the cumulative infiltration curve measured with a disc infiltrometer. The Haverkamp infiltration model is widely used to estimate S and K_s. This model includes as inputs the constants β and γ and the difference between the initial, θ_i, and final, θ_s, volumetric water contents, $\Delta\theta$. Since $\Delta\theta$ would be expressive of the possible measurement errors, and assuming β, γ, and θ_i as known values, the first objective of this work is to analyze the influence of θ_s on the optimization of K_s and S. To this end, a sensitivity analysis, which consists of estimating K_s and S for a range of θ_s was applied on synthetic infiltration curves simulated for homogeneous columns of sand and loam soil. Then, and working on real soils under different tillage management, we evaluated different procedures to measure θ_s and analyzed its impact on K_s and S estimation. Four different techniques were compared: the gravimetric-core method and two TDR invasive (3 and 5 cm) and a non-invasive (NiP) probes. All TDR probes were connected to a low-cost NanoVNA. The sensitivity analysis showed that θ_s, K_s and S can be optimized simultaneously from the inverse analysis of an infiltration curve when β and γ are known values and the infiltration curve is near the steady-state zone. However, due to the intrinsic complexities of real soils and the fact that β and γ are unknown variables, we recommended to optimize K_s and S using measured θ_s. The NiP sensor connected to a NanoVNA provided a fast, inexpensive, clean, accurate and robust alternative to measure θ_s at the end of the infiltration experiments.

1. Introduction

The characterization of the hydraulic properties of the soil surface (sorptivity, S, and hydraulic conductivity, K) is of paramount importance to solve many hydrological and environmental issues linked to soil water storage and transport in the vadose zone. These soil properties can be estimated from the inverse analysis of the transient cumulative infiltration curves measured with a tension disc infiltrometer (Angulo-Jaramillo et al., 2000, 2016), which can works from unsaturated to saturated conditions. The tension disc infiltrometer (Perroux and White, 1988) consists of a base disc attached to a graduated water supply reservoir and a bubble tower that can impose a negative pressure head at the base disc. The diameter of the disc base can range from the 25 cm proposed by Perroux and White (1988) to the 3.2 cm used by Madsen and Chandler (2007). The correct use of the tension disc infiltrometer requires the membrane of the disc base to be completely in contact with the soil surface. To achieve this contact, a thin layer of sand is commonly placed between the soil surface and the disc base. The cumulative infiltration curve is determined from the decrease of the water level inside the reservoir.

The 1D analytical solution, QEI, of Haverkamp et al. (1994) combined with the term of Smettem et al. (1994) for disk infiltrometer measurements is one of the most widely used models for estimating hydraulic properties. (e.g. Lassabatere et al., 2009; Latorre et al., 2015; Fernandez-Galvez et al., 2019). This model involves the following parameters: K_s, S, the radius of the disc, r_d, the β and γ constants, and the soil water content increase $\Delta\theta$, the latter defined as the difference between the initial, θ_i, and final, θ_s, soil volumetric water contents. While β

* Corresponding author.
E-mail address: david@eead.csic.es (D. Moret-Fernández).

https://doi.org/10.1016/j.geoderma.2024.117089
Received 11 January 2024; Received in revised form 15 October 2024; Accepted 28 October 2024
Available online 16 November 2024

is related to the soil diffusivity, $D(\theta)$, and the soil hydraulic conductivity functions, γ is a function of the approximate estimation of sorptivity (Fuentes et al., 1992; Haverkamp et al., 1994; Smettem et al., 1994).

Given that direct formulations are more convenient than complex implicit equations, Haverkamp et al. (1994) proposed using the simplified two-Terms (2T) expansion. However, since this approximation remains valid only for short to intermediate infiltration times, Moret-Fernández et al. (2020) suggested estimating K_s and S using the more accurate three-Term (3T) and four-Term (4T) expansions of the QEI model, valid over longer time intervals (Yilmaz et al., 2022). Although the QEI and 4T models have four degrees of freedom, and theoretically have the potential to estimate S, K_s, β and γ, Latorre et al. (2018) and Moret-Fernández et al. (2020) demonstrated that, assuming $\Delta\theta$ as a known value, estimation of K_s and S from transient infiltration curves requires using fixed and known β and γ values. This is explained by the fact that K_s, β and γ are closely linked through the second term of the 4T expansion, which makes that, at short-medium infiltration term, these three parameters cannot be simultaneously optimized. On the other hand, Lassabatere et al. (2009) and Yilmaz et al. (2023) showed that the β and γ depend on the type of soil and the initial water condition, and suggested that these parameters for relatively dry soils can be approximated from soil textural characteristics. In summary, according to previous studies, K_s and S are optimized variables, β and γ are approximated from soil textural properties, r_d is a measurable input, and $\Delta\theta$ is a parameter to be measured. However, despite the progress in evaluating K_s, S, β and γ, the influence of $\Delta\theta$ on the estimation of K_s and S remains uninvestigated.

The θ_s and θ_i values used in the Haverkamp et al. (1994) - Smettem et al. (1994) model are commonly obtained by gravimetric measurements, using the core method (Grossman and Reinsch, 2002). The volumetric water content, θ, is calculated as the product between the gravimetric water content, W, and the soil bulk density, ρ_b. While W is calculated as the difference between the wet and dry weight of a soil sample, ρ_b is the ratio between the dry weight and the corresponding volume of the sampled core. Although the core procedure is taken as the reference method, the feasibility of this technique for measuring θ_s at the end of a disc infiltration experiment could be questionable by different reasons. For example, the insertion of a core in saturated soil may favor soil compaction, and thus alter the estimate of θ_s. In contrast, an underestimation of θ_s is obtained if, for instance, the depth of the wetting front advance is less than the total height of the employed soil core. Although this limitation could be solved by using thinner cores, the representativeness of ρ_b decreases with very narrow cores. In addition to the fact that soil management in saturated soil conditions is cumbersome, the core method requires a further laboratory processing with the use of ovens and balances. Lastly, some authors suggest equating the saturated water content to the soil porosity, easily accessible from the dry bulk density; however, this calculation requires an adequate estimation of the specific density of soil particles, having also the problem that it may include trapped air in saturated soils (Fayer and Hillel, 1986).

As alternative, the soil volumetric water content can be measured by indirect dielectric methods, such as the Time Domain Reflectometry, TDR, technique, a non-destructive method that also allows real-time measurements of water content. Determination of θ is based on the time required by an electrical signal to travel and reflect back along the probe's rods (Topp et al., 1980). Another advantage of the TDR technique is the simplicity of the probes, which allows to design and manufacture own probes. This great versatility allows, for example, to make discontinuous probes for soil water profiles (Topp et al., 1982), soil sensors to measure the matrix water potential (Wraith and Or, 1999) or the electrical conductivity of the soil water solution (Moret-Fernández et al., 2012) or non-invasive probes (Selker et al., 1993; Persson and Berndtsson, 1998). The non-invasive sensors are especially suitable for soil surface measurements, since they allow rapid measurements without disturbing the soil surface (Persson and Berndtsson, 1998). This would be the case, for example, for the measurement of water content in the soil surface crust. Selker et al. (1993) presented a first design of noninvasive TDR, in which the two probe rods were partially embedded in a serpentine pattern within an acrylic pad. This design was further improved by Persson and Berndtsson (1998), who longitudinally inserted a three-rod TDR probe into a polyvinyl chloride (PVC) block, so that the surface of the rod surrounded half of the measurement volume. Nissen et al. (2003) studied the spatial sensitivity of two- and three-rod probes placed horizontally through the walls of an experimental box, and found that two-rod instead of three-rod probes should be used if sharp changes in ε_a are expected in the direction transverse to the plane containing the probe rods, owing to separation of the traveling electromagnetic waves in the three-rod case. These same authors reported that horizontal probe orientation is more appropriate for monitoring across sharp vertical boundaries, such as wetting fronts.

Since its first application for θ measurements in the 1980s, the TDR technology has evolved towards more portable and accurate instruments. This is the case, for example, of the evolution from heavy and bulky 1502C Metallic Cable Tester (Tektronix of Beaverton, Oregon) to the small, rugged and portable TDR100 (Campbell Scientific). However, although these new developments make the TDR technique more portable, the high cost of the TDR instruments ($\cong$ 4000 €) may limit their use in some scenarios. To overcome this limitation, Qiwei et al. (2019) proposed to measure θ using a small size and low-cost mini vector network analyzer (miniVNA). This technique was later improved by Moret-Fernández et al. (2022) who, using a low-cost FDR-TDR devices NanoVNA ($\cong$ 60 €), from 50 kHz to 1.5 GHz, allowed accurate measurements of θ.

Since $\Delta\theta$ is a critical input for optimizing K_s and S, the first objective of this paper is to conduct a sensitivity analysis to determine the influence of $\Delta\theta$ on K_s and S estimations. In the following and working on soils under different tillage systems, we evaluated different procedures to measure θ_s and analyzed its impact on K_s and S estimation. Four different techniques were compared: the gravimetric-core method and two TDR invasive (3 and 5 cm) and a non-invasive (NiP) probes.

2. Theory

2.1. Cumulative infiltration curve

The quasi-analytical 3D cumulative infiltration curve, I_{3D}, QEI, for disc infiltrometer measurements and final saturation soil conditions can be described as (Haverkamp et al., 1994; Smettem et al. 1994):

$$\frac{2(K_s-K_i)^2}{S^2}t=\frac{2}{1-\beta}\frac{(K_s-K_i)\left(I_{3D}-K_it-\frac{\gamma S^2}{r_d(\theta_s-\theta_i)}t\right)}{S^2}-\frac{1}{1-\beta}ln\left[\frac{1}{\beta}exp\left(\frac{2\beta(K_s-K_i)\left(I_{3D}-K_it-\frac{\gamma S^2}{r_d(\theta_s-\theta_i)}t\right)}{S^2}\right)+\frac{\beta-1}{\beta}\right] \quad (1)$$

where t is the time [T], S is the sorptivity [L $T^{-0.5}$], K_i and K_s [L T^{-1}] are the hydraulic conductivity values corresponding to initial, θ_i, and saturation, θ_s, volumetric water contents [L^3 L^{-3}], β is the integral shape parameter [-], γ [-] is a proportionality constant that accounts for the correction of the wetting front shape (Smettem et al., 1994) and r_d is the radius of the disc [L]. Yilmaz et al. (2023) proposed a simple relationship to estimate β and γ parameters based on soil textural classes.

The implicit Eq. (1) for negligible initial hydraulic conductivity can

Table 1
Theoretical values of initial (θ_i), saturated (θ_s) and residual (θ_r) water content, α and n parameters of the van Genuchten (1980) water retention curve, saturated hydraulic conductivity (Ks), sorptivity, S and γ and β parameters of the synthetic soils.

	θ_i	θ_r	θ_s	α	n	K_s	S [a]	β [b]	γ [b]
		$cm^3\ cm^{-3}$		cm^{-1}		$cm\ s^{-1}$	$cm\ s^{-0.5}$	-	-
Sand	0.045	0.045	0.43	0.145	2.68	$8.25\ 10^{-3}$	0.1521	0.53	1.03
Loam	0.078	0.078	0.43	0.036	1.56	$2.88\ 10^{-4}$	0.0367	1.25	0.76

[a] Moret-Fernández et al. (2017).
[b] Lassabatere et al. (2009).

be simplified to a 4-Term expansion according to (Moret-Fernández et al., 2020):

$$I_{3D}(t) = St^{\frac{1}{2}} + \left(\frac{2-\beta}{3}K + \frac{\gamma S^2}{r_d(\theta_s-\theta_i)}\right)t + \frac{K^2}{9S}(\beta^2-\beta+1)t^{\frac{3}{2}} + 2(\beta-2)(\beta+1)\frac{(1-2\beta)}{135}\frac{K^3}{S^2}t^2 \quad (2)$$

This expression is valid for long infiltration times (between 2000 and > 50000 s for coarse and fine soil textures, respectively). For short-intermediate infiltration data, Eq. (1) reduces to a 2-Term expansion (Haverkamp et al., 1994):

$$I_{3D}(t) = St^{\frac{1}{2}} + \left(\frac{2-\beta}{3}K + \frac{\gamma S^2}{r_d(\theta_s-\theta_i)}\right)t \quad (3)$$

For long-term behavior Eq. (1) gives the following result:

$$I_{3D}(t) = \left(K_s + \frac{\gamma S^2}{r_d(\theta_s-\theta_i)}\right)t + \frac{S^2}{2(K_s-K_i)(1-\beta)}ln\left(\frac{1}{\beta}\right) \quad (4)$$

2.2. Time Domain Reflectometry

In Time Domain Reflectometry, a fast-rise step voltage electromagnetic pulse is propagated in the medium along a transmission line. The cable tester records a TDR signal expressed by the reflection coefficient as a function of time. The transit time, t_L [T], of the TDR pulse propagating one return trip in a transmission line (e.g., TDR probe) of length L [L] can be approached (Topp et al., 1980) as:

$$t_L = \frac{2L\sqrt{\varepsilon_a}}{c} \quad (5)$$

where ε_a is the apparent dielectric constant and c (3 x 10^8 m/s) is the speed of light constant. The t_L value is calculated as the difference between the time at which the signal enters the TDR probe's rods (first peak) and the time when the trace arrives at the end of the TDR probe (second reflection point). This last point is calculated with the widely accepted tangent method (Heimovaara, 1993). Once t_L value is obtained, ε_a is calculated from Eq. (5).

For the case of a non-invasive TDR probe, Maheshwarla et al. (1995) showed that the measured effective apparent dielectric constant, ε_{eff}, of a TDR probe placed between two semi-infinite media with different ε_a values (ε_{a1} and ε_{a2}) can be expressed as:

$$\varepsilon_{eff} = \frac{\varepsilon_{a1}+\varepsilon_{a2}}{2} \quad (6)$$

In Eq. (6) the subscript refers to the materials, i.e., either 1 or 2. For the particular case of a TDR probe, in which the longitudinal half of the rods are covered by a block of known dielectric constant, ε_b, the ε_a value when the block is placed on a soil surface is calculated as (Persson and Berndtsson, 1998):

$$\varepsilon_a = 2\varepsilon_{eff} - \varepsilon_b \quad (7)$$

where ε_{eff} is calculated from Eq. (5).

Once ε_a is obtained, θ can be calculated by using the Topp et al. (1980) function:

$$\theta = -5.3{\cdot}10^{-2} + 2.92{\cdot}10^{-2}{\cdot}\varepsilon_a - 5.5{\cdot}10^{-4}{\cdot}{\varepsilon_a}^2 + 4.3{\cdot}10^{-6}{\cdot}{\varepsilon_a}^3 \quad (8)$$

3. Material and methods

3.1. Influence of Δθ on estimation of K_s and S: sensitivity analysis

This numerical experiment aims to evaluate whether $\Delta\theta$ can be estimated from the inverse analysis of an infiltration curve simulated in a homogeneous soil column. To this end, numerically generated data to eliminate uncertainties associated with real-world experimental errors was used. Assuming β and γ as known values, the sensitivity analysis consisted on optimizing K_s and S for a range of θ_s values and infiltration curves of different lengths. Taking a relatively homogeneous initial water content (θ_i) throughout the topsoil layer, and the ease of measuring θ_i with gravimetric or dielectric methods, θ_i was set as a known value and the analysis focused only on variations of $\Delta\theta$, derived in changes in final water content (θ_s).

The sensitivity analysis was conducted on synthetic infiltration curves generated with the HYDRUS-3D model (Šimunek et al., 1999). Water retention curves were characterized according to the van Genuchten (1980) model with Mualem condition. The curves were generated on homogeneous sand and loam soil columns (Table 1) (Carsel and Parrish, 1988). The soil volume was discretized as a cylinder (radius of 25 cm and depth of 25 cm), covering the axisymmetric plane with a 2-D rectangular mesh of 100 x 900 cells. The base of the disc infiltrometer of 10 cm radius was represented as a constant pressure head boundary on the corresponding cells, whereas the rest of the soil surface was treated as atmospheric boundary with no flux. The initial soil water content was very close to the residual water content. More details about the infiltration curve generated with HYDRUS-3D can be found in Latorre et al. (2015).

The sensitivity analysis consisted of calculating the differences between the HYDRUS-3D synthetic infiltration curve and the infiltration curves simulated with the 4-Terms expansion, Eq. (2), once the S and K_s were optimized for different values of θ_s. In all cases, β, γ (Table 1), θ_i and r_d (10 cm), Eq. (2), were assumed as known values. The inverse analysis was performed using the Levenberg-Marquardt (More, 1978) optimization algorithm. Once the S and K_s were optimized for a given value of θ_s, the error or objective function, Q, that represents the difference between the actual, I_i, and the simulated infiltration curves, $I(S, K_s, \theta_s)$, was calculated as

$$Q = \frac{\sqrt{\sum_{i=1}^{N}\left[(I_i - I(S,K_s,\theta_s))\Delta t\right]^2}}{N-1} \quad (9)$$

where N is the number of measured (I, t) values. The sensitivity analysis was applied to three infiltration curves of increasing times: 500, 3000, and 6000 s for the loam column and 75, 150, and 250 s for sand. $\Delta\theta$ values explored a range of ±10% around the actual θ_s, with 1% increments. Finally, for each combination of θ_s and infiltration time, the analysis identified the minimum Q value (indicating the best fit) and the corresponding optimal K_s and S.

Table 2
Rod diameter, ϕ_r, separation of external rods, S_r, and effective length, L, of the three different TDR probes used in the infiltration experiment to measure the saturated water content.

	ϕ_r	S_r	L
		mm	
P3	1	10	30
P5	2	20	50
NiP	5	20	78.5

3.2. Field experiments

In this section, we first describe the TDR probes that were used to measure θ_s at the end of an infiltration experiment, which protocol is described in following sections.

3.2.1. TDR probes

Three TDR probes of different geometries were compared: two three-rod TDR probe of (i) 3 cm, P3, and (ii) 5cm, P5, lengths, respectively and (iii) a two-rod non-invasive TDR probe, NiP. The geometries of the different probes are summarized in Table 2.

A different manufacturing process was employed in P3 and P5. While the external and central rods of P3 were directly welded to the inner terminal and connector housing of a female-BNC connector, the corresponding rods in P5 were directly welded to the central cable and the external mesh of a coaxial cable, respectively. For the case of P5, the head of the TDR probe was completely coated with epoxy and the end of the coaxial cable was welded to a male-BNC connector. Measurements of soil water content with P3 and P5 were performed by vertically inserting the probes into the soil.

The NiP probe consisted of two rods inserted longitudinally into a circular Teflon block of 10 cm radius and 1.9 cm thickness, so that half of the rod surface was contained in the Teflon block. Both rods were placed in the central part of the Teflon block, such that 1 cm of Teflon protruding from each end of the probe. One end of each of the rods was welded to the central cable and the external mesh of a coaxial cable, respectively, which end was welded to a male-BNC connector. However, while the depth explored by the 3-rod TDR probes is clearly defined by the length of the TDR wires vertically inserted into the soil, the measured depth allowed by NiP is more confusing. To clarify this uncertainty, the theoretical volume explored by NiP was calculated numerically following the procedure outlined in Nissen et al. (2003). The cross-section probe geometry electrostatic problem was solved by finite elements analysis with a commercial software (COMSOL Multiphysics) in a 1m x 1 m domain. The sensitivity function was then computed and integrated to estimate the probe volume sensitivity.

3.2.2. FDR-TDR instrument

The volumetric water content was measured by connecting the different TDR probes to a low-cost Vector Network Analyzers (VNA) commercially available (NanoVNA), with 1.5 GHz maximum operating frequency (Owotech, 2019; Moret-Fernández et al., 2022). The NanoVNA can be used for measurements of Frequency Domain Reflectometry (FDR) or, after suitable postprocessing, for TDR measures. Although TDR and FDR are dual procedures, TDR procedure was selected because it is easier to interpret for soil experiments. According to Moret-Fernández et al. (2022), the time resolution of this device is approximately 0.333 ns. Although the relatively low frequency supplied by this device limits the number of points per TDR waveform, previous experiments demonstrated that this instrument can be satisfactorily employed as a TDR cable tester for measuring the volumetric water content in soils (Moret-Fernández et al., 2022). The NanoVNA was connected to a smart mobile phone, that allowed downloading the FDR signal using the free available NanoVNA WebApp (https://play.google.com/store/apps/details?id=net.lowreal.nanovnawebapp&hl=es_PA&pli=1). The FDR signal was then transformed to the time domain using Fast Fourier Transform (FFT) and Inverse Fast Fourier Transform (IFFT) efficient algorithms (Moret-Fernández et al., 2022). Given that the recorded TDR signal presents a limited density of points (100 points per signal), the waveforms were interpolated up to 2400 points using a cubic interpolation method. Once the TDR signal was obtained, θ was calculated according to procedure described in section 2.2. The use of the Topp et al. (1980), Eq. (8), was accompanied by a previous calibration experiment.

The NanoVNA device was calibrated following the Open-Short-Load standard calibration procedure (Sayed and Martens, 2013) with the assistance of the NanoVNA firmware. Finally, the effective length of the different TDR probes was determined by immersing the corresponding TDR probes in distilled water, and comparing the water dielectric constant measured at known temperature with the corresponding

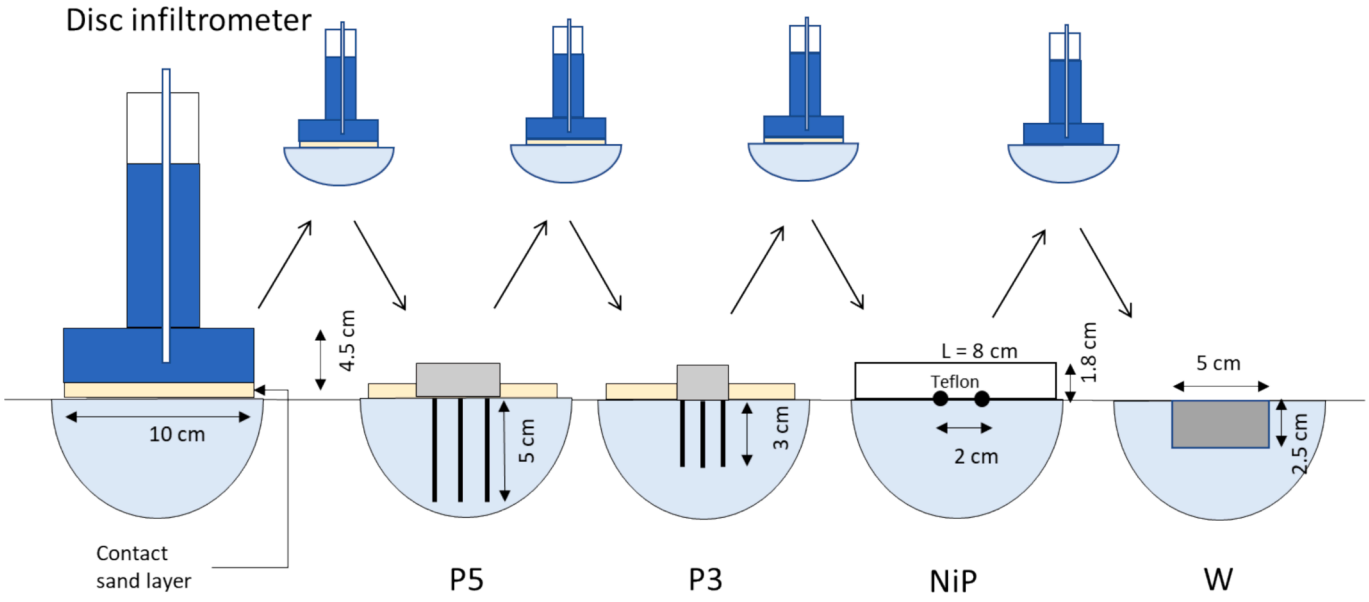

Fig. 1. A schematic of the procedure used to measure the volumetric water content at the saturated soil surface using the three-rod TDR probes of 5 cm, P5, and 3 cm, P3, long, the no-invasive probe without contact sand layer, NiP, and the core method, W.

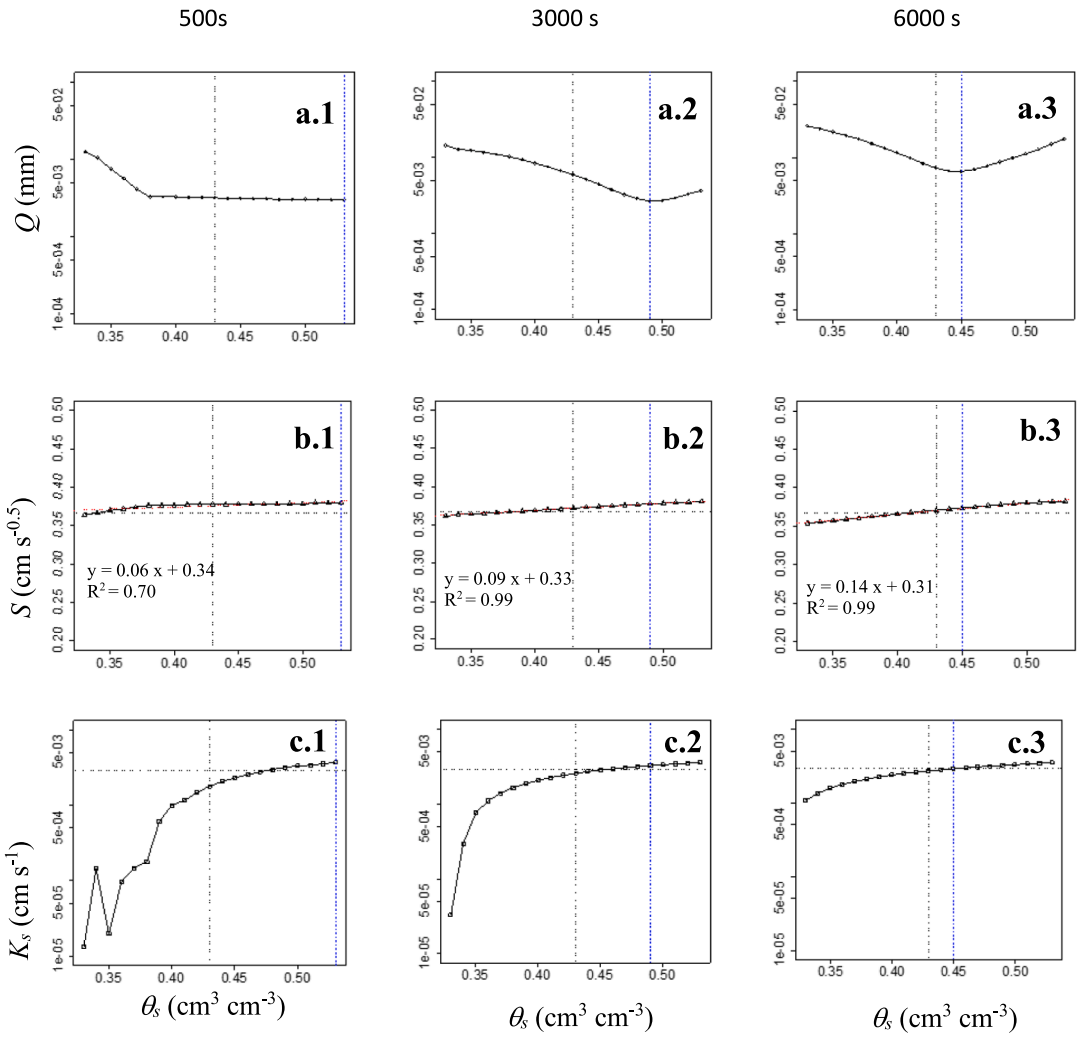

Fig. 2. Relationship between the saturated volumetric water content θ_s and (a) the objective function, Q, Eq. (9), (b) the sorptivity, S, and (c) the saturated hydraulic conductivity, K_s, estimated from the inverse analysis of a synthetic infiltration curve simulated in a loam soil column, at infiltration times of 500, 3000 and 7000 s of, respectively. The dashed grey lines indicate the theoretical values of θ_s, K_s and S, and vertical blue lines are the optimized θ_s. The red dashed line in Fig. 2a.2, 2b.2 and 2c.2 is the regression line between θ_s and S.

theoretical value (Jones et al., 2002). This calibration experiment was also used to check the shape of the TDR signals when the P3, P5 and NiP probes were immersed in water.

3.2.3. *Infiltration experiments and θ_s measurements*

The different TDR probes designed for water content measures at the end of an infiltration were tested in nine infiltration experiments. To this end, the θ_s measured with the different TDR probes inserted in the saturated soil at the end of the infiltration were compared with the corresponding water content measured gravimetrically using the core method, θ_{s_w}. A schematic of the procedure is summarized in Figure 1

The infiltration experiments were performed on a dryland research farm of the Estación Experimental de Aula Dei (CSIC) in the province of Zaragoza (latitude 418440N; longitude 08460W; altitude 270 m). Soil at the research site is a loam (fine-loamy, mixed thermic Xerollic Calciorthid) according to the USDA soil classification (Soil Survey Staff, 1975). Selected physical and chemical properties of the soil for this layer were given in López et al. (1996). The measurements were conducted in April 2023, in three adjacent and nearly level plots (slope 0–2%). The plots were in the fallow period of a winter barley (*Hordeum vulgare* L.) - fallow rotation. Three different soil tillage managements were considered: conventional tillage (CT), reduced tillage (RT) and no-tillage (NT). While CT consisted of moldboard ploughing of fallow plots, RT used chisel ploughing as primary tillage. NT used exclusively herbicides (glyphosate) for weed control throughout the fallow season.

The initial water content of the soil, θ_i, was in all cases lower than 0.1 cm^3 cm^{-3}. Within each plot, three infiltration measurements were performed. A compact design of tension disc infiltrometer (10 cm diameter and height) was used, where the water level drop was monitored by a smartphone camera (Latorre et al., 2021). A thin contact sand layer, with a thickness between 1 to 2 mm, was placed between the disc base and the soil surface (Perroux and White, 1988). The offset calculated for the contact sand layer (Reynolds, 2006) was less than 2 mm. The sand was levelled using a leveler or methacrylate tube closed at the bottom, with the same diameter and height as the infiltrometer. Excess sand outside the leveler base was removed. The tension at the disc base was fixed to 0 cm. Assuming that water content of the dry topsoil layer was homogeneously distributed, θ_i was measured with TDR by vertically inserting the P5 probe right next to the infiltration point.

After filling the infiltrometer with water, the smartphone was positioned in front of the leveler to capture the entire reservoir on its screen. Camera distance and angle were adjusted to ensure a clear focus. Video recording was then initiated. The leveler was swiftly replaced with the water-filled disc infiltrometer, marking the start of infiltration time.

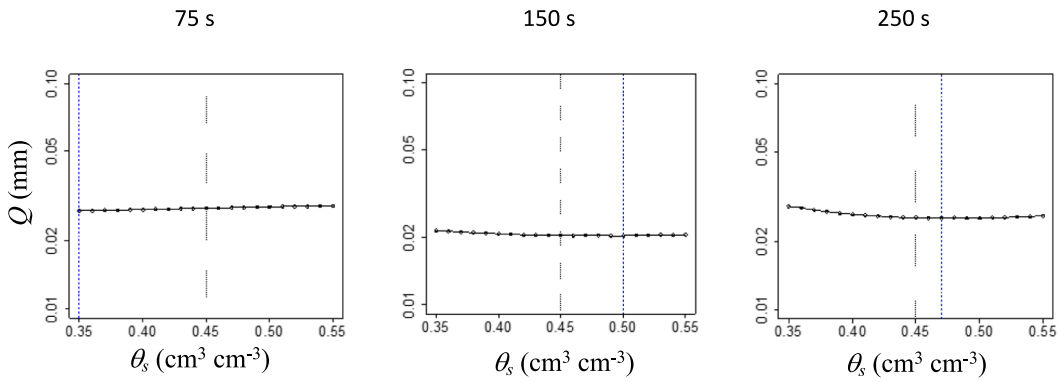

Fig. 3. Relationship between the saturated volumetric water content θ_s and the objective function, Q, Eq. (9), estimated from the inverse analysis of a synthetic infiltration curve simulated in a sand column, at infiltration times of 75, 150 and 250 s of, respectively. The dashed grey lines indicate the theoretical values of θ_s, and vertical blue lines are the optimized θ_s.

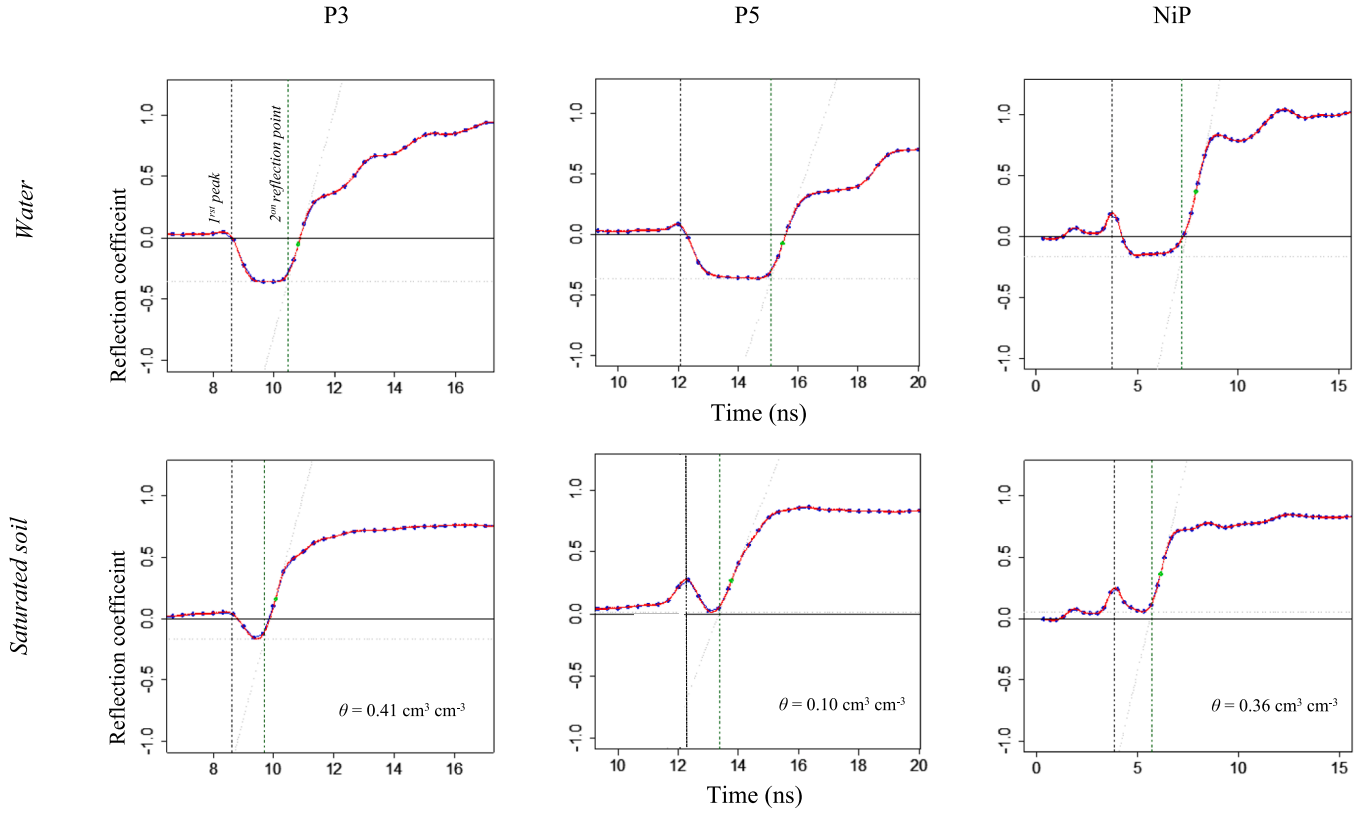

Fig. 4. TDR waveforms measured with the 5 cm, P5, and 3 cm, P3, long three-rod TDR probes and the no-invasive probe, NiP, when immersed in distilled water and inserted in the saturated soil sampled in replication one of the reduced tillage treatment.

Infiltration proceeded until approximately 30 mm of water had infiltrated. At this point, the video recording was stopped. Following the procedure outlined by Latorre et al. (2021), each video was used to generate an experimental infiltration curve. At the end of the infiltration experiment, the infiltrometer was lifted off the soil surface and the P5 probe, which was previously connected to the NanoVNA plus smartphone, was inserted three times into the soil, inside the sand layer circumference, but making sure that the probe head went completely through the sand layer and that the rods were fully inserted into the soil matrix. During each insertion, a FDR signal was recorded. This process took less than 10 s. In order to replenish the drained water during TDR measurements, at the end of the TDR measurements the infiltrometer was placed again on the sand layer for 2 minutes. After this time, the procedure applied to P5 was repeated for the P3 probe. After P3 measurements, the infiltrometer was again lifted off the soil, and the sand layer was removed with a masonry trowel. Immediately after, the NiP probe was placed on the bare and saturated soil, and the FDR signal was recorded. This process took less than 5 s. After that, the infiltrometer was placed again on the bare soil for 2 minutes. Finally, the infiltrometer was again lifted off and a stain steel cylinder (2.5 cm height and 5 cm diameter) was inserted on the center of the saturated circumference. The core was next extracted, the excess of soil removed and the sample poured into plastic flask with airtight closure.

Once in the laboratory, the TDR waveforms were download and analyzed. The collected cores were weighted, dried at 105 °C and reweighted to obtain the gravimetric saturated water content of the soil, W_s. The volumetric saturated water content obtained gravimetrically, θ_{s_w}, was calculated as the product of W_s and the soil bulk density, ρ_b, the

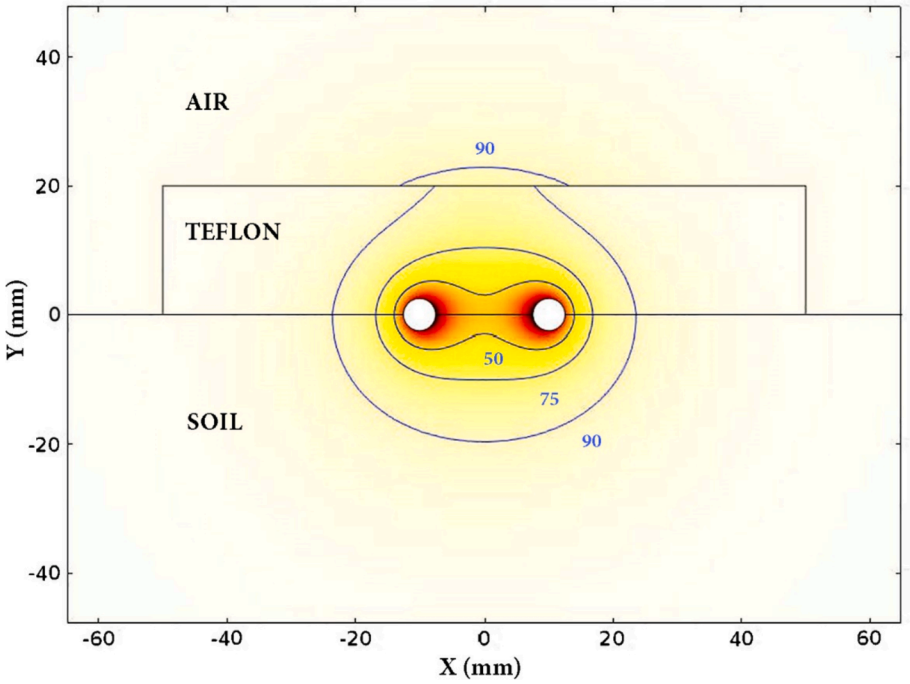

Fig. 5. Sensitivity distribution of NiP two-rod probe (colored) and sample areas containing 50%, 75% and 50% of the total sensitivity.

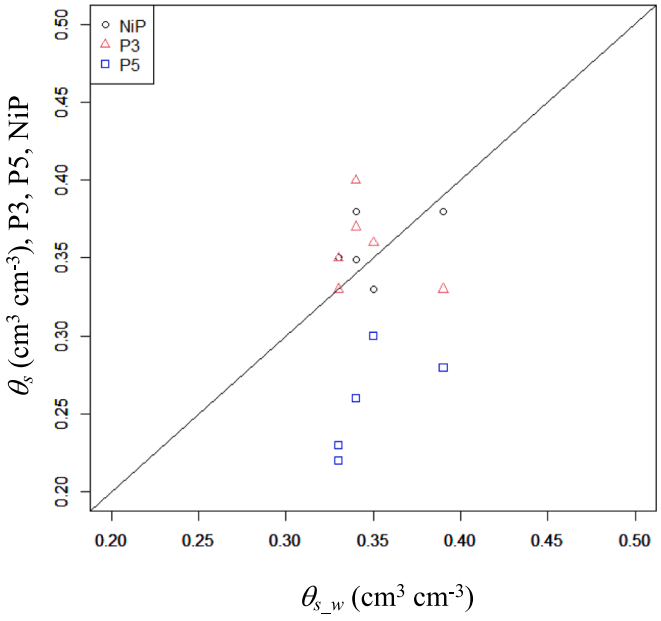

Fig. 6. Relationship between the saturated volumetric water content measured with the core method, θ_{s_w}, and corresponding values, θ_s, measured with the 5 cm, P5, and 3 cm, P3, long three-rod TDR probes and the no-invasive probe, NiP, at the different sampling points.

latter calculated as the ratio of W_s to the cylinder volume. After a first visual inspection of the data and the absence of extreme values, for simplicity, the arithmetic mean and standard deviation of the replicates were used to obtain a representative value for each treatment as well as the intrinsic variability of the measurements and analysis. To evaluate the accuracy of the TDR probes, the relative error (RE) was calculated as the quotient between the θ_s values measured by the TDR probes (θ_s) and the gravimetric reference values (θ_{s_w}). In addition, an analysis of variance (ANOVA) was performed between the θ estimated by the different procedures.

Table 3
Average, standard deviation and relative error, *RE*, of the volumetric water content measured on the infiltration experiments using the core method, W, method, the three-rod P3 and P5 TDR probe and the non-invasive, NiP, TDR sensor. Rows with the different letter indicate significant differences ($p < 0.05$) between treatments.

Treatment	*Average*	*Standard deviation*	*RE*
	cm^3 cm^{-3}		%
W	0.345 **a**	0.021	-
P3	0.362 **a**	0.025	4.9
P5	0.232 **b**	0.058	-33.0
NiP	0.356 **a**	0.015	3.2

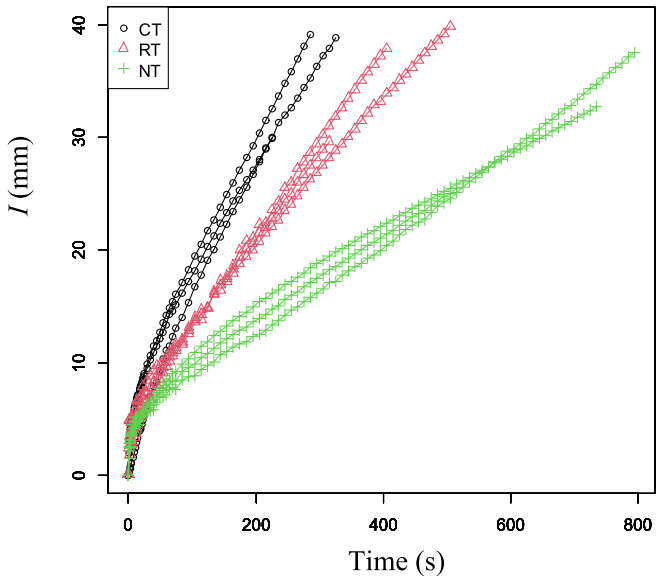

Fig. 7. Infiltration curves measured in the conventional tillage, CT, reduced tillage, RT, and, no-tillage, NT, treatments.

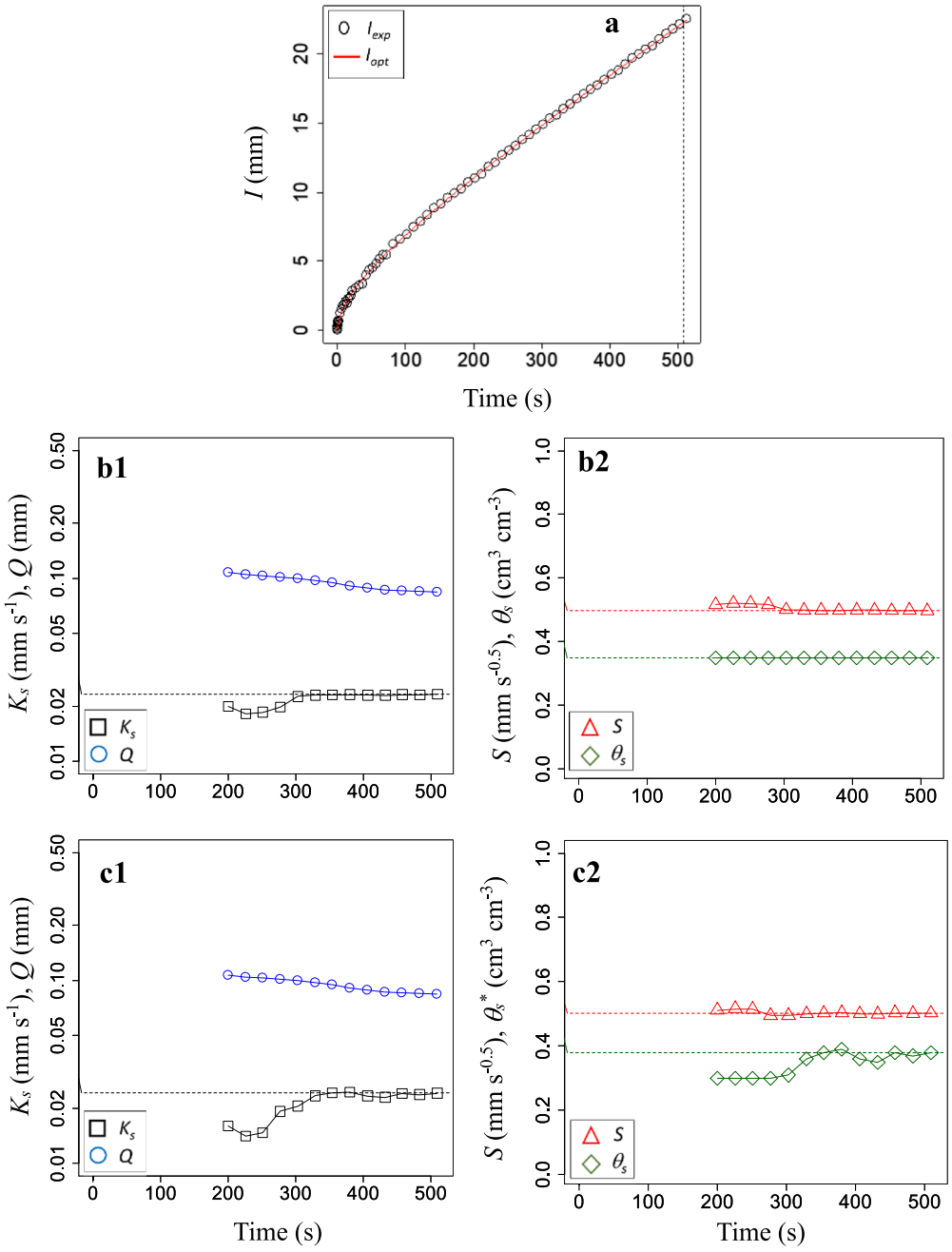

Fig. 8. (a) Experimental, I_{exp}, and optimized, I_{opt}, infiltration curves measured in the third replication of the no-tillage treatment, and time evolution of the saturated hydraulic conductivity, K_s, sorptivity, S, saturated volumetric water content, θ_s, and the objective function for the infiltration curve, Q, optimized with SIA method using (b) the measured volumetric water content, θ_s, and (c) the optimized water content, θ_s*. Horizontal dashed lines are the respective theoretical values K_s, S and θ_s.

Using the SIA procedure (Moret-Fernández et al., 2021), the S, K_s and the optimal infiltration time, t_o, were estimated from the inverse analysis of the measured infiltration curve. The optimization process involved two consecutive sequential analyses. In a first step, the effect of the contact sand layer on the inverse analysis was removed using Latorre et al. (2015) procedure. The sand effect was considered as a gap, in time and volume, before water infiltrates into the soil, and the contact sand layer influence was removed by finding the sand infiltration time, t_{sand}, (and its corresponding water volume) and shifting the experimental data to the origin. In a next step, the optimization of S and K_s as function of θ_s was performed using the Sequential Infiltration Analysis (SIA) procedure (Moret-Fernández et al., 2021). The SIA method estimates S and K_s of the upper soil layer by fitting the 4-Term expansion, Eq. (2), to increasing infiltration time series, and computes the objective function Q, Eq. (9), as a function of the number of data points considered. A total of 20 increasing times were considered. The t_o is defined as the time with a minimum Q value, and the actual S and K_s are the corresponding values calculated for an infiltration curve of time t_o. The Levenberg-Marquardt (More, 1978) optimization algorithm was used in the inverse analysis. The γ and β parameters were fixed to 0.75 and 1.25, respectively, which correspond to the theoretical values for a loam soil (Lassabatere et al., 2009).

Table 4
Average soil sorptivity, S, saturated hydraulic conductivity, K_s and objective function, Q, Eq. (7), calculated within the optimum infiltration time, t_o, using the volumetric water content, θ_s, measured with non-invasive TDR probe, and the corresponding values obtained using the optimized volumetric water content, θ_s*. Data within the parentheses denotes the standard deviation. CT, RT and NT indicate conventional tillage, reduces tillage and no tillage, respectively.

	Measured θ_s					Optimized θ_s*				
	θ_s	S	K_s	Q	t_o	θ_s*	S	K_s	Q	t_o
	cm^3cm^{-3}	mm $s^{-0.5}$	mm s^{-1}	mm	s	cm^3cm^{-3}	mm $s^{-0.5}$	mm s^{-1}	mm	s
CT1	0.35	0.60 (0.015)	0.044 (0.006)	0.19 (0.014)	277	0.38 (0.04)	0.61 (0.042)	0.042 (0.015)	0.19 (0.014)	277
CT2	0.38	0.80 (0.004)	0.048 (0.002)	0.22 (0.016)	378	0.35 (0.03)	0.79 (0.010)	0.045 (0.004)	0.22 (0.016)	378
CT3	0.38	0.67 (0.013)	0.053 (0.002)	0.16 (0.002)	301	0.37 (0.05)	0.66 (0.081)	0.052 (0.004)	0.16 (0.002)	301
RT1	0.36	0.69 (0.000)	0.141 (0.000)	0.19 (0.000)	50	0.31 (0.00)	0.68 (0.000)	0.140 (0.000)	0.19 (0.000)	50
RT2	0.35	0.92 (0.030)	0.047 (0.009)	0.09 (0.005)	230	0.31 (0.03)	0.89 (0.032)	0.045 (0.011)	0.08 (0.055)	230
RT3	0.37	1.00 (0.004)	0.037 (0.003)	0.09 (0.005)	157	0.32 (0.00)	1.00 (0.003)	0.019 (0.003)	0.09 (0.005)	157
NT1	0.33	0.60 (0.003)	0.001 (0.001)	0.16 (0.008)	720	0.37 (0.01)	0.63 (0.003)	$3.8\ 10^{-4}$ ($2\ 10^{-4}$)	0.14 (0.006)	720
NT2	0.35	0.35 (0.004)	0.028 (0.001)	0.17 (0.006)	240	0.34 (0.05)	0.38 (0.001)	0.027 (0.002)	0.17 (0.006)	240
NT3	0.35	0.50 (0.000)	0.022 (0.002)	0.09 (0.008)	509	0.34 (0.04)	0.50 (0.006)	0.021 (0.004)	0.09 (0.008)	509

To evaluate the influence of θ_s on the optimization process, the SIA procedure was first applied using the measured θ_s, and then applied on a simultaneous optimization of S, K_s and θ_s (taking θ_s as unknown value), whose optimized θ_s was defined as θ_s*. The S and K_s estimated with both procedures were compared with each other, and the optimized θ_s* was then compared with the measured θ_s. Since this paper is not focused on to compare tillage systems, no statistical analysis was performed among tillage treatments.

4. Results and discussion

4.1. Influence of $\Delta\theta$ on estimation of K_s and S: sensitivity analysis

The sensitivity analysis showed that infiltration time has an effect on the estimation of θ_s, K_s and S (Fig. 2). Overall, the flat shape observed in the θ_s vs Q relationship within the interval [$\theta_s \pm 10\%$] and infiltration time of 500 s (Fig. 2a.1) indicates that similar infiltration curves can be obtained for different values of θ_s. On the other hand, the optimized θ_s (blue vertical line in Fig. 2a.1) was far from its theoretical value. The limited sensitivity observed in short infiltration curves can be explained with the 2-Term expansion, Eq. (3). This model, while valid for short to intermediate infiltration times, might not fully account for all the relevant processes governing infiltration, particularly for longer durations. The interdependence between the three optimized parameters existing in the second term of Eq. (3) implies that similar infiltration curves can be obtained for different combinations of S, K_s and θ_s. Similarly, the interdependence between γ, β and K_s within the 2-T expansion explains why optimization of K_s at medium infiltration times also requires taking γ and β as fixed values. Overall, an increasing relationship was observed between θ_s and the optimized S and K_s. However, while a linear relationship, with relatively small slope, was observed between θ_s and S (Fig. 2b.1), a more abrupt behavior was found for K_s (Fig. 2c.1). The analysis revealed that variations in K_s were larger for θ_s below the theoretical value compared to scenarios where θ_s exceeded the theoretical value. These findings suggest that when optimizing S and K_s using short-to-intermediate infiltration curves, it is crucial to treat θ_s as a known value. This is particularly important for experimental measurements, as soil heterogeneity often makes it difficult to obtain perfectly homogeneous infiltration curves with sufficiently long durations.

The behavior observed for short-intermediate infiltration curves changed significantly with increasing infiltration times, where the θ_s vs. Q relationship for longer infiltrations (e.g. 3000 and 600 s) exhibited a clearer and unique minimum (Fig. 2a.2 and 2a.3). In this case, longer infiltration times enabled the optimized θ_s to converge closer to its theoretical value. These results could be explained by the additional coefficients of the 4-Term expansion, Eq. (2), which compensate for the parameter interaction described in the 2-Term model, Eq. (3), and allows optimizing an additional variable. The results suggest that the closer is the infiltration time to the steady-state, Eq. (4), simultaneous and more accurate estimates of θ_s, K_s and S can be achieved (Fig. 2). For example, this hypothesis is supported by the sensitivity analysis obtained in the sand column (Fig. 3), where, compared to loam soil, significantly shorter infiltration times (e.g. 250 s) allowed accurate optimization of θ_s. Thus, these results indicate that optimization of θ_s depends on how close the infiltration time is to the steady-state region. However, due to the interdependence between $\Delta\theta$, γ and β within the steady-state zone, Eq. (4), these three parameters cannot be simultaneously estimated with Eq. (4), since different combination of them results in similar steady-state curves. Thus, given that β and γ are approximate values obtained from the soil textural characteristics, to reduce the uncertainty in the optimization of K_s and S, as far as possible, it is preferable to estimate K_s and S from measured values of $\Delta\theta$. As observed in short-intermediate infiltration curves, an increasing relationship was observed between θ_s and the optimized S and K_s (Fig. 2b and c). However, the dispersion of K_s within the [$\theta_s \pm 10\%$] interval decreased as infiltration times approached to the steady-state zone. In conclusion, these results indicate that optimization of S and K_s is not very sensible to θ_s when the total infiltration time is close to its steady-state.

4.2. Field experiments

4.2.1. TDR probes

Overall, the temporal resolution of the NanoVNA connected to P3, P5 and NiP was enough to characterize the dielectric constant of water (Fig. 4), where the well-defined shape of the TDR waveform allows detecting the first peak and the second reflection point. For example, for the most restrictive case of P3, seven points were defined between the first peak and the second reflection point. Although detection of first peak and second reflection point is maintained when the probes are inserted in saturated soil, the low number of points obtained in P3 (between 3 and 4) would probably be at the limit for accurate estimation of water content (Fig. 4). However, this is not the case of NiP, where the number of points within these time intervals doubles with respect to P3. The low number of points found in P5 inserted in saturated soil (Fig. 4) is due to the fact (as will be described in section 4.2.1) that the soil at the time of the measurement was not saturated.

The simulated soil volume explored with NiP showed that the 90% curve of total sensitivity reaches 2 cm depth into the soil. However, although the 90% curve has a leakage of 3 mm outside the Teflon support in the air region, and therefore, the ε_a value obtained with Eq. (6) is underestimated, the deviation for the expected ε_a in saturated soils is less than 0.5%, and can be neglected. Thus, the results showed that the volume explored with NiP extends 2.5 cm to each side of the probe center and reaches 2 cm below the soil surface along the probe length (Fig. 5).

In conclusion, although the results suggest that P3 connected to a NanoVNA device is not a priori a consistent design for measuring the

water content of a saturated soil, NiP and P5 may in principle be suitable geometry probes for measuring the soil water content at the end of an infiltration experiment at saturated soil conditions.

4.2.2. θ mesurements

The mean and standard deviation of θ_i measured on the field with P5 was 0.04 and 0.02 cm^3 cm^{-3}, respectively. Statistical analysis showed that only P5, which tended to underestimate θ_s (Fig. 6) and presented a relative error, *RE*, of 33%, was significantly different to θ_{s_w} (Table 3). These results were due to the fact that the wetting front at the time of measurement probably did not exceed the 5 cm length of the P5 inserted vertically into the soil. Thus, these results indicate that care must be taken in choosing the length of the sensor to measure the soil water content. Although this problem could be solved by inserting the probes obliquely, this alternative introduces the question of what is the optimal angle of insertion. Alternatively, limitations of P5 could also be solved by extending the infiltration times, for which infiltrometers with a larger water reservoir should be needed. Thus, all these restrictions suggest that P5 inserted vertically into the soil is not the best suitable probe for measuring soil moisture in infiltration experiments performed with a portable and compact infiltrometer,

In contrast, P3 and NiP sensors exhibited good agreement (Fig. 5) and similar average values were found between θ_{s_w} and the corresponding θ_s values measured with TDR (Table 3). In this case, the *RE* for P3 and NiP was acceptable and, in both cases, lower than 5% (Table 1). However, the low number of points obtained in the P3-TDR waveform, with only 3 to 5 points from the first peak to the second reflection point (Fig. 4), makes it difficult to locate the singular points of the TDR waveform and, consequently, to accurately estimate soil water content. This problem is partially minimized with NiP, which, between the first peak and the second reflection point, has more than three time as many points as P3. Another advantage of NiP over P3 is that a single measurement of NiP scan a larger volume (Fig. 5) than P3, for which 3 replicates were taken per sampling point. The use of the NiP probe also means faster measurements, which reduces the influence of the drainage process on the water content measurements. On the other hand, the NiP probe explores a significantly larger soil volume than that obtained with the gravimetric method. While the gravimetric method samples a cylindrical volume of 2.5 cm depth and 5 cm diameter, the NiP probe integrates a larger horizontal half-elliptical cylinder measuring 8 cm long with 2.5 cm and 2 cm horizontal and vertical half-axes, respectively. Thus, the slight dispersion between θ_{s_w} and the θ_s values measured with NiP could be attributed to the different volume explored by the two methods.

4.2.3. Hydraulic properties estimation

Figure 7 shows all infiltration curves measured in field, where maximum and minimum infiltrations corresponded to CT and NT, respectively. Based on the superior performance of NiP probes for measuring θ_s, from now on, all optimizations with known θ_s will be performed using the θ_s measured by NiP.

Figure 8 shows the time evolution of the optimized Q, K_s and S over an experimental infiltration curve using the measured θ_s (Fig. 8b) and an optimized θ_s* (Fig. 8c). In all cases, S showed minimal changes over time (Fig. 8b2 and c2), which indicates that this parameter is little affected by θ_s (Fig. 2). However, different behavior was found in K_s, where the K_s optimized using the measured θ_s (Fig. 8b1) was more stable over time than that obtained by simultaneous optimization with θ_s* (Fig. 8c1). These results highlight the importance of optimizing K_s using measured values of $\Delta\theta$, especially for short infiltration experiments. The high infiltration rate of this soil (Fig. 8a), which resulted in a rapid approach to steady-state, may explain the accurate estimates of S, K_s, and θ_s* for relatively short infiltration times. As shown in Figure 8a, the curve shows a linear trend towards the end of the experiment, suggesting the infiltration process is approaching steady-state.

Overall, robust and significant relationships ($R^2 = 0.99$, $p < 0.0001$) with slope close to one were obtained in all field infiltrations between the S, K_s and Q values within t_o optimized using the measured θ_s and those obtained using the optimized θ_s*. Within each experimental infiltration curve, a same t_o was obtained with both optimization procedures (Table 4). In addition, similar mean values and standard deviation of S, K_s and Q, were obtained when these variables were optimized using θ_s and θ_s* (Table 4). A different behavior, however, was observed on the volumetric water content ($R^2 = 0.01$; $p = 0.81$; $y = -0.15x + 0.399$), where the average θ_s (0.36 cm^3 cm^{-3}) was 10% larger than θ_s* (0.34 cm^3 cm^{-3}). These results would suggest that S and K_s could be, in principle, calculated from θ_s*. However, given the greater variability observed in K_s optimized with θ_s* (Fig. 8), together with the uncertainties promoted by the unknowns γ and β, the uncertainty of the infiltration time in real soils and the fact that θ_s can be easily measured with the NiP plus NanoVNA system, we conclude that, as far as possible, it is preferable to optimize the soil hydraulic properties using a measured volumetric water content.

5. Conclusion

This study investigates the influence of $\Delta\theta$ on estimating K_s and S through inverse analysis of 3D infiltration curves. Taking β and γ as known values, the sensitivity analysis revealed that simultaneous optimization of $\Delta\theta$, K_s and S can be achieved when the total infiltration time approaches steady-state conditions. However, since real soils generally exhibit some heterogeneity, it is preferable to optimize K_s and S based on a measured $\Delta\theta$ value. Following a comparison of various TDR sensors for measuring θ_s (volumetric water content) and θ_i (initial water content), the results suggest that non-invasive TDR probes connected to a low-cost NanoVNA offer a viable alternative for direct θ_s measurements. The high portability and rapid measurements facilitated by this combination of non-invasive probes and NanoVNA could be a significant advancement for accurate estimation of soil hydraulic properties. However, further efforts should be done, for instance, to evaluate alternative non-invasive TDR probes for direct measurements of the soil water content without removing the contact sand layer.

CRediT authorship contribution statement

D. Moret-Fernández: Validation, Supervision, Resources, Methodology, Investigation, Formal analysis, Data curation, Conceptualization. **F. Lera:** Supervision, Methodology, Formal analysis, Conceptualization. **D. Yilmaz:** Supervision, Conceptualization. **L. Lassabatere:** Supervision, Data curation, Conceptualization. **J.J. Jiménez:** Writing – review & editing, Project administration, Funding acquisition. **B. Latorre:** Supervision, Software, Methodology, Investigation, Conceptualization.

Declaration of competing interest

The authors declare that they have no known competing financial interests or personal relationships that could have appeared to influence the work reported in this paper.

Acknowledgments

This research was partially supported by the RENURSE project (ref. TED2021-132406B-I00).

Data availability

Data will be made available on request.

References

Angulo-Jaramillo, R., Bagarello, V., Iovino, M., Lassabatere, L., 2016. Infiltration measurements for soil hydraulic characterization, Infiltration Measurements for Soil

Hydraulic Characterization. Springer, Switzerland. https://doi.org/10.1007/978-3-319-31788-5.
Angulo-Jaramillo, R., Vandervaere, J.P., Roulier, S., Thony, J.L., Gaudet, J.P., Vauclin, M., 2000. Field measurement of soil surface hydraulic properties by disc and ring infiltrometers. A review and recent developments. Soil Tillage Research 55, 1–29.
Carsel, R.F., Parrish, R.S., 1988. Developing joint probability distributions of soil water retention characteristics. Water Resour. Res. 24, 755–769.
Fayer, M.J., Hillel, D., 1986. Air encapsulation: I. Measurement in a field soil. Soil Sci. Soc. Am. J. 50, 568–572.
Fernandez-Galvez, J., Pollacco, J.A.P., Lassabatere, L., Angulo-Jaramillo, R., Carrick, S., 2019. A general Beerkan Estimation of Soil Transfer parameters method predicting hydraulic parameters of any unimodal water retention and hydraulic conductivity curves: Application to the Kosugi soil hydraulic model without using particle size distribution data. Adv. Water Resour. 129, 118–130.
Fuentes, C., Haverkamp, R., Parlange, J.-Y., 1992. Parameter constraints on closed-form soilwater relationships. J. Hydrol. 134, 117–142.
Grossman, R.B., Reinsch, T.G.. 2002. Bulk density and linear extensibility. In Dane, J.H., and G.C. Topp. Eds. Methods of soil analysis, Part. 4. SSSA. Madison, WI. pp. 201-254.
Haverkamp, R., Ross, P.J., Smettem, K.R.J., Parlange, J.Y., 1994. Three dimensional analysis of infiltration from the disc infiltrometer. Part 2. Physically based infiltration equation. Water Resour. Res. 30, 2931–2935.
Heimovaara, T.J., 1993. Design of triple-wire time domain reflectometry probes in practice and theory. Soil Sci. Soc. Am. J. 57, 1410–1417.
Jones, S.B., Wraith, J.M., Or, D., 2002. Time domain reflectometry principles and applications. Hydrol. Process 16, 141–153.
Lassabatere, L., Angulo-Jaramillo, R., Soria-Ugalde, J.M., Simunek, J., Haverkamp, R., 2009. Numerical evaluation of a set of analytical infiltration equations. Water Resour. Res. 45. https://doi.org/10.1029/2009WR007941.
Latorre, B., Peña, C., Lassabatere, L., Angulo-Jaramillo, R., Moret- Fernández, D., 2015. Estimate of soil hydraulic properties from disc infiltrometer three-dimensional infiltration curve. Numerical analysis and field application. J. Hydrol. 57, 1–12.
Latorre, B., Moret-Fernández, D., Lassabatere, L., Rahmati, M., López, M.V., Angulo-Jaramillo, R., Sorando, R., Comín, F., Jiménez, J.J., 2018. Influence of the β parameter of the Haverkamp model on the transient soil water infiltration curve. J. Hydrol. 564, 222–229.
Latorre, B., Moret-Fernández, D., Lyons, M.N., Palacio, S., 2021. Smartphone-based tension disc infiltrometer for soil hydraulic characterization. J. Hydrol. 600, 126551.
López, M.V., Arrúe, J.L., Sánchez-Girón, V., 1996. A comparison between seasonal changes in soil water storage and penetration resistance under conventional and conservation tillage systems in Aragón. Soil Till. Res. 37, 251–271.
Madsen, M.D., Chandler, D.G., 2007. Automation and use of mini disk infiltrometers. Soil Science Soc. Am. J. 71, 1469–1472.
Maheshwarla, S.V., Venkatasubramanian, R., Boehm, R.F., 1995. Comparison of Time Domain Reflectometry Performance Factors for Several Dielectric Geometries: Theory and Experiments. Water Resour. Res. https://doi.org/10.1029/95WR00788.
More, J.J., 1978. The Levenberg-Marquardt algorithm: implementation and theory. In: Watson, G.A. (Ed.), Lecture Notes in Mathematics 630: Numerical Analysis. Springer-Verlag, Berlin, pp. 105–116.
Moret-Fernández, D., Vicente, J., Aragüés, R., Peña, C., López, M.V., 2012. A new TDR probe for measurements of soil solution electrical conductivity. J. Hydrol. 448–449, 73–79.
Moret-Fernández, D., Latorre, B., López, M.V., Pueyo, Y., Lassabatere, L., Angulo-Jaramilo, R., Rahmati, M., Tormo, J., Nicolau, J.M., 2020. Three-and four-term approximate expansions of the Haverkamp formulation to estimate soil hydraulic properties from disc infiltrometer measurements. Hydrol. Process. 34, 5543–5556. https://doi.org/10.1002/hyp.13966.
Moret-Fernández, D., Latorre, B., Lassabatere, L., Di Prima, S., Castellini, M., Yilmaz, D., Angulo-Jaramillo, R., 2021. Sequential infiltration analysis of infiltration curves measured with disc infiltrometer in layered soils. J. Hydrol. 600, 126542.
Moret-Fernández, D., Lera, F., Latorre, B., Tormo, J., Revilla, J., 2022. Testing of a commercial vector network analyzer as low-cost TDR device tomeasure soil moisture and electrical conductivity. Catena 218, 106540.
Nissen, H.H., Ferré, P.A., Moldrup, P., 2003. Sample area of two- and three-rod time domain reflectometry probes. Water Resour. Res. 39. https://doi.org/10.1029/2002WR001303.
OwOTech, 2019. NanoVNA V2 (S-A-A-2)- 4GHz vector network analyzer (VNA) capable of measuring antennas, filters, duplexers, and amplifiers. GitHub repository.
Perroux, K.M., White, I., 1988. Designs for disc permeameters. Soil Sci. Soc. Am. J. 52, 1205–1215.
Persson, M., Berndtsson, R., 1998. Noninvasive water content and electrical conductivity laboratory measurements using time domain reflectometry. Soil Sci. Soc. Am. J. 6.
Qiwei, Z., Zainuddin, M.F., Ahmad, A.F., Obays, S.J., Abbas, Z., 2019. Development of an affordable soil moisture sensor system with mini-VNA tiny and smartphone. Sci. Technol 27, 1121–1129.
Reynolds, W.D., 2006. Tension infiltrometer measurements: implications of pressure head offset due to contact sand. Vadose Zone J. 5, 1287–1292. https://doi.org/10.2136/vzj2006.0098c.
Sayed, M., Martens, J., 2013. Vector network analyzers. In: Teppati, V., Ferrero, A., Sayed, M. (Eds.), Modern RF and Microwave Measurement Techniques (The Cambridge RF and Microwave Engineering Series). Cambridge University Press, Cambridge, pp. 98–129.
Selker, J.S., Graff, L., Steenhuis, T., 1993. Noninvasive time domain reflectometry moisture measurement probe. Sci. Soc. Am. J. 57, 934–936.
Šimunek, J., Šejna, M., van Genuchten, M.-T., 1999. The HYDRUS-2D Software Package for Simulating the Two-dimensional Movement of Water, Heat, and Multiple Solutes in Variably-saturated Media. Version 2.0. U.S. Salinity laboratory. Agricultural Research Service, USDA, Riverside, California.
Smettem, K.R.J., Parlange, J.Y., Ross, P.J., Haverkamp, R., 1994. Three-dimensional analysis of infiltration from the disc infiltrometer, 1, A capillary-based theory. Water Resour. Res. 30.
Soil Survey Staff. 1975. Soil taxonomy: a basic system of soil classification for making and interpreting soil surveys. USDASCS Agric. Handbook 436. US Govt. Print. Office, Washington, DC.
Topp, G.C., Davis, J.L., Annan, A.P., 1980. Electromagnetic determination of soil water content: Measurements in coaxial transmission lines. Water Resour. Res. 16, 574–582.
Topp, G.C., Davis, J.L., Annan, A.P., 1982. Electromagnetic determination of soil water content using TDR: II. evaluation of installation and configuration of parallel transmission lines. Soil Sci. Soc. Am. J. 46, 678–684.
Van Genuchten, M.T., 1980. A closed form equation for predicting the hydraulic conductivity of unsaturated soils. Soil Sci. Soc. Am. J. 44, 892–898.
Wraith, J.M., Or, D., 1999. Soil water characteristic determination from concurrent water content measurements in reference porous media. Soil Sci. Soc. Am. J. 65, 1659–1666.
Yilmaz, D., Di Prima, S., Stewart, R.D., Abou Najm, M.J., Fernandez-Moret, D., Latorre, B., Lassabatere, L., 2022. Three-term formulation to describe infiltration in water-repellent soils. Gerderma. 427. https://doi.org/10.1016/j.geoderma.2022.116127.
Yilmaz, D., Lassabatere, L., Moret-Fernandez, D., Rahmati, M., Angulo-Jaramillo, R., Latorre, B., 2023. Soil-dependent β and γ shape parameters of the Haverkamp infiltration model for 3D infiltration flow. Hydrol. Process. 37. https://doi.org/10.1002/hyp.14928.